Film-forming amines adsorption and corrosion kinetics on carbon steel surface in neutral solution investigated by EIS and PM-IRRAS analysis

Deni Jero, Nicolas Caussé, Olivier Marsan, Thierry Buffeteau, Fabrice Chaussec, Amaury Buvignier, Marion Roy, Nadine Pébère

Electrochimica Acta xxx (xxxx) 141925

Contents lists available at ScienceDirect

Electrochimica Acta

journal homepage: www.elsevier.com/locate/electacta

Film-forming amines adsorption and corrosion kinetics on carbon steel surface in neutral solution investigated by EIS and PM-IRRAS analysis

Deni Jero [1,2,3,*], Nicolas Caussé [1], Olivier Marsan [1], Thierry Buffeteau [4], Fabrice Chaussec [2], Amaury Buvignier [2], Marion Roy [3], Nadine Pébère [1,*]

[1] Université de Toulouse, CIRIMAT, UPS/INPT/CNRS, ENSIACET 4, Allée Emile Monso-CS 44362, 31030 Toulouse cedex 4, France
[2] ODYSSEE Environnement-Service R&D, Belle Croix, 72510 Requeil, France
[3] Université Paris-Saclay, CEA-Service d'Etude du Comportement des Radionucléides, 91191, Gif-sur-Yvette, France
[4] Université de Bordeaux, ISM, UMR 5255 CNRS, 351 Cours de la Libération, 33405 Talence, France

ARTICLE INFO

Article history:
Received 30 November 2022
Received in revised form 9 January 2023
Accepted 18 January 2023

Keywords:
Corrosion inhibitor
Neutral electrolyte
Adsorption kinetics
Inhibition efficiency
EIS
Raman Spectroscopy
PM-IRRAS

ABSTRACT

N-oleyl-1, 3-propanediamine (OLDA) is one of the most used film-forming amines (FFAs) for the corrosion protection of carbon steel circuits of a wide range of industrial plants. The present work focused on the study of OLDA adsorption kinetics onto the carbon steel surface by electrochemical impedance spectroscopy (EIS). The diagrams were obtained in a 200 $mg.kg^{-1}$ NaCl with and without OLDA for immersion times ranging from 2 min to 140 min and for two temperatures (25°C and 50°C). It was shown that, from the beginning of immersion (2 min), OLDA adsorption and corrosion occurred simultaneously on the carbon steel surface. With increasing immersion time, a dynamic and competitive process between both phenomena was established until a steady-state was reached and the corrosion was slowed down. *Ex situ* Raman spectroscopy analyses revealed a heterogeneous distribution of the OLDA molecules on the surface with a preferential adsorption on the corrosion products, mainly γ-FeOOH. E*x situ* Polarization Modulation Infrared Reflection Absorption Spectroscopy (PM-IRRAS) analyses confirmed the formation of mixed barrier layers (OLDA molecules/corrosion products) whose thickness increased with time and temperature.

1. Introduction

The use of film-forming amines (FFAs) as corrosion inhibitors is an advantageous route for the corrosion protection of carbon steel circuits of a wide range of industrial plants from boilers to secondary circuits of nuclear pressurized water reactors. In neutral/alkaline and aerated electrolytes, carbon steel corrosion is described by the following anodic (1) and cathodic (2) reactions leading to the formation of iron oxides and/or hydroxides [1]:

$$Fe \rightarrow Fe^{2+} + 2e^{-} \quad (1)$$

$$O_2 + 2H_2O + 4e^{-} \rightarrow 4HO^{-} \quad (2)$$

The corrosion products can partly accumulate on the carbon steel surface or can be transported by water through the circuits. The main roles of FFAs treatment are first, to reduce corrosion and as a consequence, to limit corrosion products transport in continuous operation and secondly, to protect the plants from corrosion during shutdown/layup periods [2]. Industrial feedbacks testify the positive effects of FFAs treatment [3–6].

Upon injection in the circuits, the amine functions of FFAs molecules bind to the metal or iron oxides/hydroxides surfaces leaving the alkyl chain pointing outwards preventing corrosive species, such as water and oxygen, to reach the substrate. Although it has been shown that FFAs form protective barriers against corrosion [7–8], several aspects need to be investigated: FFAs adsorption mechanism on the oxides/hydroxides, barrier thickness and morphology and in particular the FFAs adsorption and desorption kinetics. The study of these different aspects would help to improve existing protocols of carbon steel surface pretreatments as well as the quantity of FFAs injected in the circuits and their injection frequency.

The specificity of FFAs is attributed to the affinity of the amine functions with the metallic surfaces and oxides. Several studies support the hypothesis of chelates or mixed layers formed between the FFAs and the iron oxides. Topp *et al.* [9] have studied the effect on FFAs on the growth of the iron oxide layers at 196°C by Confocal Laser Scanning Microscopy (CLSM). They found that the organic film did not impede the oxide layer formation but it was thinner and more uniform. Mao *et al.* [10] noted that at 75°C in a deaerated acetate solution, the FFAs molecules were combined with iron corrosion products to form a "compact, composite outer layer-inhibitor barrier". Liu *et al.* [11] have shown that

* Corresponding authors.
E-mail addresses: deni.jero@toulouse-inp.fr (D. Jero), nadine.pebere@ensiacet.fr (N. Pébère).

https://doi.org/10.1016/j.electacta.2023.141925
0013-4686/© 20XX

the FFAs adsorption on α-Fe_2O_3 particles, synthesized by hydrothermal routes, delayed their growth and thus forming smaller particles.

Until recently, FFAs protective barrier was often described as a monolayer [2]. However, Baux *et al.* [7–8] have determined FFAs thickness of 10-20 nm on carbon steel/magnetite surfaces, by *in situ* electrochemical impedance spectroscopy (EIS) measurements, suggesting higher values than that of a monolayer. Jäppinen *et al.* [12] have determined thicknesses dependent on temperature by using *ex situ* Glow-Discharge Optical Emission Spectroscopy (GDOES) depth profiles. The FFA barrier thickness has been estimated to 40 nm at 228°C and 120 nm at 300°C. More recently, Yoshioka *et al. [13]* have determined a FFAs thickness of 500 nm on copper (Cu) surface by Nuclear Magnetic Resonance (NMR). They attributed the stacking of FFAs molecules to their complexation with the Cu ions.

The FFAs adsorption and desorption kinetics study would be of great interest to better control their injection frequency in circuits [14]. Only few papers have reported the FFAs adsorption during experiments. To quantify the FFAs adsorption, the residual FFAs concentration in the solution over immersion time has been determined with the Bengal-Rose method [15–16]. Jack *et al.* [15] have determined first-order deposition constant and a first-order release constant of FFAs labile layers. Cuoq *et al.* [16] have concluded that the FFAs adsorption behaviour was linked to thermal gradient on the steel substrate. However, to understand the FFAs adsorption kinetics onto metallic surface, the surface changes over immersion time should be monitor *in situ* and in real time.

Electrochemical Impedance Spectroscopy (EIS) is one of the most used *in situ* techniques at laboratory scale to assess inhibition efficiency of organic compounds [17–20]. Several studies have shown that EIS can also be a reliable technique for the *in situ* study of Self Assembled Monolayers (SAMs) adsorption kinetics onto gold surfaces [21–24] and pre-oxidized surfaces, such as copper [25–26]. EIS presents several advantages over used techniques for the study of adsorption kinetics, such as quartz microbalance (QCM) [27–28], ellipsometry or Surface Plasmon Resonance (SPR) [29–30]. While EIS allows the study of substrates with roughness found in industrial circuits, the mentioned techniques require controlled substrate roughness (usually very smooth surfaces). Moreover, corrosion and adsorption processes cannot be distinguished in these techniques.

The present work aims to investigate the N-oleyl-propanediamine (OLDA) adsorption kinetics onto carbon steel surfaces using EIS. The study was carried out at a fixed OLDA concentration of 100 $mg.kg^{-1}$ in a 200 $mg.kg^{-1}$ NaCl non-adjusted pH electrolyte. A protocol for the impedance spectra acquisition was established to follow the processes occurring at the carbon steel/electrolyte interface from the beginning of immersion. Thus, open circuit potential and impedance diagrams were obtained consecutively several times during two hours. Similarly, the spectra were registered in the absence of OLDA to assess the inhibition efficiency as a function of time. The electrochemical study was supplemented by *ex situ* Raman Spectroscopy and by Polarization Modulation Infrared Reflection Absorption Spectroscopy (PM-IRRAS) for a detailed analysis of the corrosion products, their interaction with OLDA and an estimation of the barrier thickness. Both the electrochemical measurements and the surface analysis were performed at 25°C and 50°C.

2. Experimental

2.1. Materials

P265GH carbon steel cylindrical rods were supplied from SMB (France) as a representative material of the water/steam industrial circuits. Its chemical composition in weight percent was as follows: C: 0.14; Mn: 1.03; Si: 0.22; Cu: 0.05; Cr: 0.04; Al: 0.04 and Fe to balance. For the electrochemical measurements, the lateral part of the steel rod was covered with a heat-shrinkable insulating sheath, leaving only the tip of the carbon steel (surface area of 1 cm^2) in contact with the solution. Before the immersion in the electrolyte, the steel surface was polished with SiC paper (grade 1200), rinsed with deionized water and dried.

For the Raman and PM-IRRAS analysis, disks of 1 cm^2 and 2 mm thick were cut from the carbon steel rod. For the Raman spectroscopy experiments, the same protocol as for the EIS measurements was applied. For the PM-IRRAS experiments, in order to achieve lower surface roughness, the substrates were further polished up to 0.25 μm with diamond paste and then with Al_2O_3 suspension. Finally, they were ultrasonically cleaned with ethanol and dried. Atomic Force Microscopy (AFM) analyses revealed a mean roughness of 24 ± 9 Å. PM-IRRAS analyses were also performed on gold substrates, purchased from Ssens (gold layer thickness of 200 nm). Before immersion in the electrolyte, the carbon steel and gold substrates were exposed to UV-ozone for 15 min in order to remove organic impurities. Then, they were fixed to the rotating disk electrode to reproduce the hydrodynamic conditions used for the EIS experiments.

N-oleyl-1, 3-propanediamine (OLDA) (Fig. 1) with a purity of 98% was supplied by ODYSSEE Environnement. All the electrochemical measurements were carried out at a concentration of 100 $mg.kg^{-1}$ in a corrosive aerated solution prepared from deionized water (18.2 MΩ cm) by adding 200 $mg.kg^{-1}$ NaCl (analytical grade). The electrolyte was chosen based on its low electrical conductivity and because it is an easily reproducible baseline solution for the electrochemical impedance measurements. The same electrolyte and conditions were used for the samples preparation for the Raman Spectroscopy and PM-IRRAS analyses. The pure OLDA molecule is little soluble in aqueous solution, in particular for the chosen concentration. In order to reach reproducible results, the NaCl solution containing the OLDA was stirred during 45 min at room temperature before each experiment.

2.2. Electrochemical impedance spectroscopy (EIS)

The electrochemical measurements were performed using a Biologic VSP-245 apparatus with a conventional three-electrode cell. The working electrode consisted of the carbon steel rod. A Red-Rod reference electrode (saturated KCl) by Radiometer Analytical was used. The counter-electrode was a large platinum grid. The working electrode rotation rate was fixed at 500 rpm. The temperature of the electrolyte was controlled at 25 ± 1°C and 50 ± 1°C by using a water circulating bath. Upon immersion of the working electrode into the electrochemical cell containing the solution (with or without OLDA), the open circuit potential (OCP) was measured during 20 s. This was followed by an impedance measurement at the OCP, under potentiostatic regulation, in the frequency range of 100 kHz to 90 mHz with 6 points per decade. A 50 mV_{rms} amplitude perturbation was applied for the experiments with OLDA and 20 mV_{rms} for those without OLDA. The linearity of the system was checked by varying the sinusoidal amplitude from 20 mV_{rms} to 50 mV_{rms}. The chosen frequency range allows both the barrier formation and the corrosion process to be described and it allows the impedance measurement time to be reduced to 2 min. The time resolution is crucial to monitor the initial steps of these processes and to ensure the stationarity of the electrochemical system during the measurement.

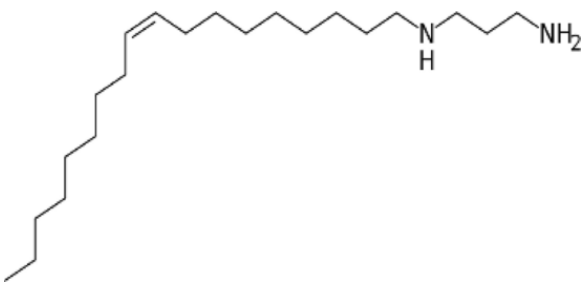

Fig. 1. Molecular structure of N-Oleyl-1,3-propanediamine (OLDA).

One cycle consisted in 20 s of OCP and an EIS measurement. It was repeated 47 times for a total immersion time of 115 min. This kinetics study was followed by 5 min of OCP and a final EIS measurement of 21 min corresponding to a frequency range from 100 kHz to 10 mHz with 8 points per decade, using a 20 mV_{rms} sinusoidal voltage. Impedance data above 10 kHz were not considered due to experimental artefacts linked to the low conductivity of the electrolyte [31].

2.3. Raman spectroscopy

Raman analyses were carried out using a confocal Raman Labram HR 800 Horiba Yvon Jobin microscope. The substrates were exposed to continuous laser radiation supplied by diode laser at 532 nm with a power of 12 mW. Attenuation filters were used to avoid any degradation of the materials. All the Raman spectra were acquired using a 600 tr/mm grating with a spectral resolution of 1 cm^{-1} and collected with a quantum well detector cooled to -60°C by double Peltier effect (CCD Synapse). The substrates were focused under a ×100 objective of an Olympus BX 41 microscope, with a numerical aperture of 0.9 giving the system a lateral resolution of 0.7 µm. The map was obtained using an XYZ motorized table with a measurement step of 2 µm. Each spectrum of the maps was acquired within a 30 s time frame and three accumulations from 200 cm^{-1} to 3500 cm^{-1}.

2.4. Polarization modulation infrared reflection absorption spectroscopy (PM-IRRAS)

PM-IRRAS spectra of OLDA films deposited onto the carbon steel or gold substrates were recorded using a ThermoNicolet Nexus 670 FTIR spectrometer at a resolution of 4 cm^{-1} by co-adding several blocks of 1500 scans (30 min acquisition time). Generally, eight blocks (4 h acquisition time) were necessary to obtain PM-IRRAS spectra of OLDA with good signal/noise ratios. Experiments were performed at an incidence angle of 75° by using an external homemade goniometer reflection attachment and adding a ZnSe photoelastic modulator (PEM, Hinds Instruments, type III) after the polarizer [32]. PM-IRRAS spectra are presented in terms of the IRRAS unit (*i.e.* 1-[Rp(d)/Rp(0)], where Rp(d) and Rp(0) stand for the p-polarized reflectance of the film/substrate and bare substrate systems, respectively) by using a calibration procedure [33]. All spectra were collected in a dry-air atmosphere.

First, IRRAS spectra were simulated for various thicknesses using the isotropic optical constants of OLDA and carbon steel (or gold [34]) according to the Abeles' matrix formalism [35–37]. The OLDA optical constants (refractive index n(ν) and extinction coefficient k(ν) in the three space directions) were experimentally determined from polarized attenuated total reflectance (ATR) spectra (data not shown) using the interdependence of n(ν) and k(ν) by the Kramers-Kronig relations as described elsewhere [38–39]. Then, from the linear dependence of the simulated IRRAS intensity of the $\nu_a CH_2$ mode versus the OLDA barrier thickness (data not shown), the experimental thicknesses were estimated.

3. Results and discussion

3.1. Monitoring OLDA adsorption and carbon steel corrosion kinetics

3.1.1. Open circuit potential (OCP)

The OCP variation of the carbon steel electrode in a 200 $mg.kg^{-1}$ NaCl solution with the OLDA inhibitor was recorded as a function of time at 25°C and 50°C (Fig. 2). For both temperatures, the first measurement was carried out during 20 s after immersion. It was followed by the registration of an EIS diagram (2 min) corresponding to the blank spaces between two OCP measurements repeated during 115 min. For both temperatures, the OCP variation during 2 min is negligible allowing the acquisition of stable EIS spectra for the chosen frequency range.

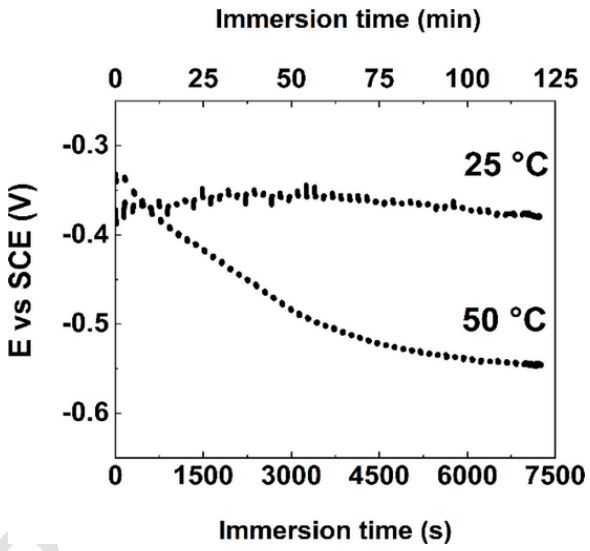

Fig. 2. OCP vs. immersion time recorded at 25°C and 50°C for the carbon steel during immersion into a 100 $mg.kg^{-1}$ OLDA / 200 $mg.kg^{-1}$ NaCl solution. Electrode rotation rate: 500 rpm.

Its variation, during the total measurement time (120 min), shows that a steady-state is reached for both temperatures. At 50°C, OCP shifts towards cathodic values with immersion time suggesting higher corrosion rate for higher temperatures, consistent with literature data [40–41].

3.1.2. EIS diagrams: influence of immersion time and temperature

Some impedance spectra (10 kHz-90 mHz) recorded from 2 min to 115 min of immersion with and without OLDA at 25°C and 50°C are reported in Fig. 3 and Fig. 4, respectively. The complete spectra (10 kHz-10 mHz) corresponding to a total immersion time of 140 min are also reported in Fig. 3 and Fig. 4. At 25°C and without OLDA (Fig. 3a), the diagrams exhibit only one time constant linked to the charge transfer process [7–8]. The decrease of the impedance modulus and phase angle from 2 min to 140 min reveals a corrosion rate increase over immersion time. In presence of OLDA, the diagrams exhibit two time constants (Fig. 3b). The first one at low frequency (from 10 Hz to 90 mHz) describes the charge transfer process, as without inhibitor. The impedance modulus and phase angle increase during the first 40 min and then slightly decline until the end of the experiment. A second time constant, from 10 kHz to 100 Hz, progressively appears over time until stabilization is reached for 140 min of immersion. In this frequency range, the time constant describes the capacitive behaviour of the adsorbed organic molecules [7–8].

At 50°C and without OLDA, the impedance spectra exhibit two time constants (Fig. 4a). The first one, from 100 Hz to 0.42 Hz, describes the charge transfer process. The second time constant at low frequency, from 0.42 Hz to 0.01 Hz, appears from about 1 h of immersion only, and is clearly visible after 140 min of immersion, when the low frequency points are recorded. This second time constant can be attributed to oxygen diffusion [42]. At constant pressure, oxygen solubility decreases as temperature increases [43–44]. At 50°C, due to the corrosion acceleration, the oxygen reduction is more limited by the diffusion process. As a result, the time constant related to the oxygen diffusion appears at 50°C and not at 25°C for the same immersion time. Moreover, when the immersion time increases, the progressive formation of corrosion products could also limit the O_2 reduction on the carbon steel surface [45]. In the presence of OLDA, the impedance spectra (Fig. 4b) show two time constants as observed at 25°C. The first time constant, from 10 Hz to 0.1 Hz, describes the corrosion activity; the impedance modulus and the phase angle decrease until their stabilization starting from 75 min of immersion. The second time constant, from 10 kHz to 100 Hz, appears

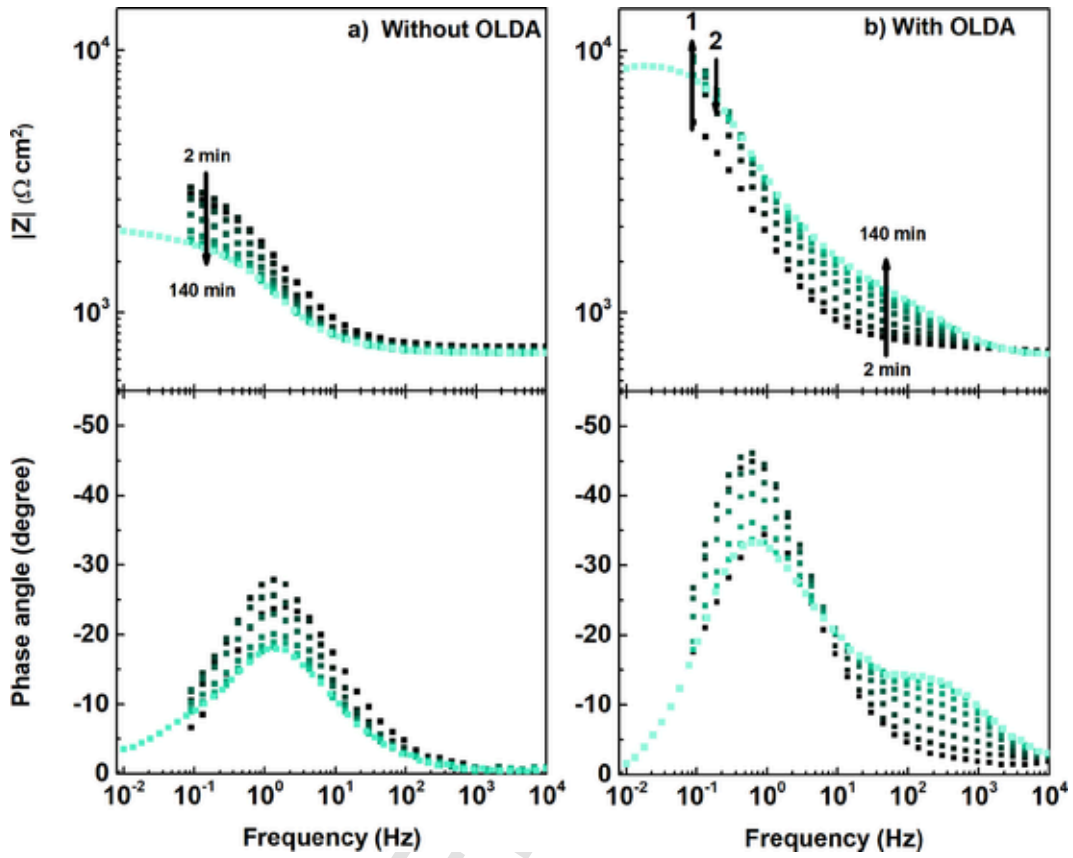

Fig. 3. EIS diagrams (Bode plots) for the carbon steel vs. immersion time starting from 2 min to 140 min of immersion at 25°C a) in a 200 mg.kg^{-1} NaCl solution without OLDA and b) in a 100 mg.kg^{1} OLDA / 200 mg.kg^{-1} NaCl solution. Electrode rotation rate: 500 rpm. Arrow 1 corresponds to the spectra from 2 min to 100 min of immersion and arrow 2 to those from 100 min to 140 min.

from 5 min of immersion; it evolves to reach a maximum and then decreases until stabilization from 75 min to the end of the experiment.

For both temperatures, the higher impedance modulus at low frequency, compared to those obtained without inhibitor, and the presence of a time constant at high frequency confirm that the OLDA adsorption on the carbon steel surface decreases its corrosion rate [7-8, 46]. Furthermore, the impedance modulus with and without OLDA at 50°C are lower than the respective values at 25°C suggesting a corrosion acceleration due to the temperature increase [40–41], in agreement with the OCP results. The impedance spectra obtained in the presence of OLDA at 25°C and 50°C indicate that two phenomena are occurring simultaneously on the carbon steel surface: the OLDA molecules adsorption and the carbon steel corrosion. Both phenomena vary over immersion time and temperature establishing a dynamic system where the OLDA adsorption competes with the carbon steel corrosion process until steady-state is reached. From the impedance spectra, two parameters were considered: the charge transfer resistance which will be used to calculate the OLDA inhibition efficiency and the OLDA barrier capacitance at high frequency. The variation of these two parameters with immersion time and temperature will be discussed further in the paper.

3.1.3. Inhibition efficiency

The inhibition efficiency, describing the ability of the molecules to slow down the corrosion rate, was calculated according to the following equation:

$$IE\ (\%) = \frac{R_{ct}^{inhibitor} - R_{ct}^{0}}{R_{ct}^{inhibitor}} \times 100\ \% \qquad (3)$$

where $R_{ct}^{inhibitor}$ and R_{ct}^{0} are the charge transfer resistances with and without inhibitor, respectively.

The charge transfer resistance (R_{ct}) values can be graphically determined at low frequency or by fitting the impedance spectra with an appropriate electrical equivalent circuit. In the present study, the graphical approach was preferred because, as it will be seen later, corrosion products and adsorbed OLDA molecules are distributed heterogeneously on the carbon steel surface. With inhibitors, the commonly used electrical equivalent circuit describes uniform protective layers [47]. This is not the case here and the system cannot be simply described with an equivalent circuit. The R_{ct} values were easily extracted from the impedance data at low frequency (impedance modulus corresponding to a phase angle close to zero). The electrolyte resistance value, determined at high frequency, was subtracted from the R_{ct} values.

The inhibition efficiencies of OLDA at 25°C and 50°C as a function of time are reported in Fig. 5. The mean R_{ct} values after 140 min of immersion and the corresponding inhibition efficiencies, calculated from several experiments, are reported in Table 1.

At 25°C, the inhibition efficiency is about 52 % for 2 min of immersion and it increases progressively until reaching a steady-state value of 84 % from 75 min of immersion to the end of the experiment. At 50°C, the inhibition efficiency starts around 50 % for 2 min of immersion and increases rapidly during the first 30 min until it reaches the maximum efficiency of about 80 %. After 30 min of immersion, the efficiency decreases and stabilizes at about 74 % due to the corrosion acceleration. Jiang *et al.* [41] have reported the same phenomenon for the OLDA inhibition efficiency on a carbon steel surface in a 37 wt. % HCl medium determined by weight loss measurements. The decrease of the inhibi-

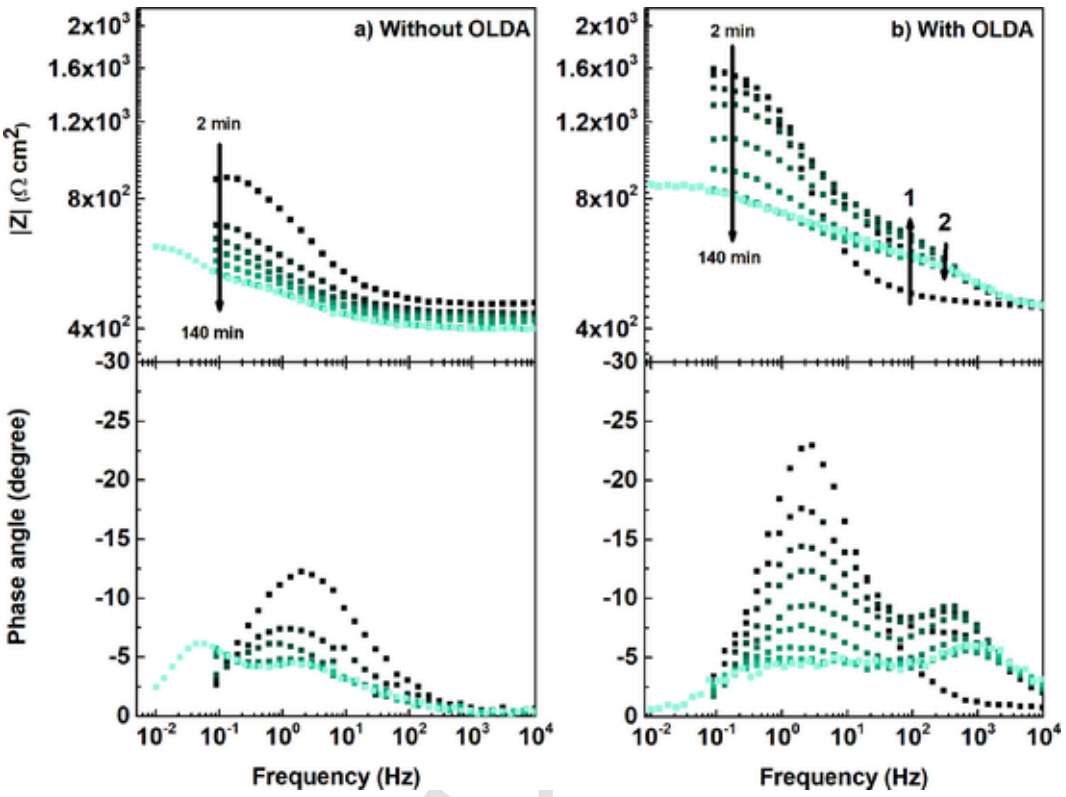

Fig. 4. EIS diagrams (Bode plots) for the carbon steel vs. immersion time starting from 2 min to 140 min of immersion at 50°C a) in a 200 mg.kg^{-1} NaCl solution without OLDA and b) in a 100 mg.kg^{-1} OLDA / 200 mg.kg^{-1} NaCl solution. Electrode rotation rate: 500 rpm. Arrow 1 corresponds to the spectra from 2 min to 75 min of immersion and arrow 2 to those from 75 min to 140 min.

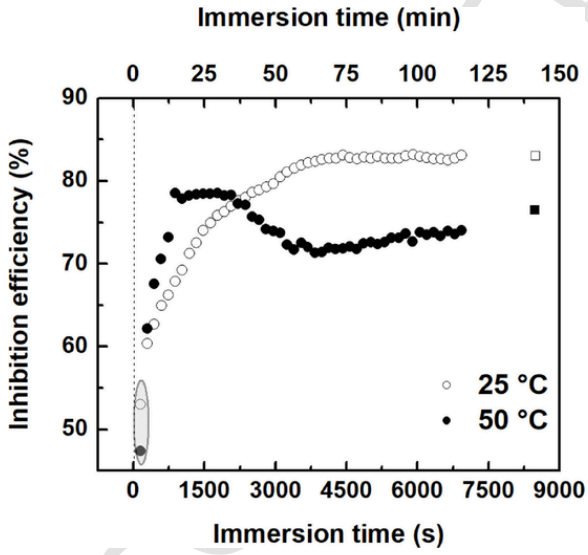

Fig. 5. OLDA inhibition efficiency as a function of time at 25°C (○) and 50°C (●). The last points correspond to the complete spectra after 140 min of immersion at 25°C (□) and 50°C (■).

tion efficiency was also attributed to the corrosion acceleration with temperature increase.

For both temperatures, from 2 min of immersion, the inhibition efficiency was about

50 % suggesting fast OLDA adsorption onto the carbon steel surface. Subramanian *et al.* [21] have noted that for concentration as high as 1 mM, alkanethiol adsorption onto gold surface was so fast that about 40 % of the surface coverage was completed within the first 500 ms.

Table 1
Mean R_{ct} values and corresponding inhibition efficiency (IE) obtained for the carbon steel after 140 min of immersion, with and without OLDA, at 25°C and 50°C, calculated from 3 to 5 experiments with the respective mean standard deviation.

		R_{ct} (Ω cm²)	IE (%)
25°C	Without OLDA	1477 ± 82	-
	With OLDA	9213 ± 1013	**84**
50°C	Without OLDA	114 ± 12	-
	With OLDA	431 ± 60	**74**

The inhibition efficiency is commonly assimilated to the surface coverage and used to determine adsorption isotherms [41]. However, in the present study, the inhibition efficiency cannot be considered as the surface coverage, only. The possible adsorption of the OLDA molecules onto the corrosion products and/or the interaction of the carbon chain of OLDA molecules should also be considered [48]. As a consequence, the data analysis with kinetics models such as Langmuir or Freundlich isotherms is not appropriate.

Ex situ carbon steel surface observations performed after different immersion times (2 min, 30 min and 140 min) and for the two temperatures (25°C and 50°C) are shown in Fig. 6. Without OLDA, corrosion products with the shape of hydrodynamic patterns are observed and their quantity increases with immersion time. After 140 min of immersion, more corrosion products can be observed on the metal surface at 50°C than at 25°C. In the presence of OLDA and for both temperatures, less corrosion products are observed suggesting a partial protection of the carbon steel surface. Furthermore, an equilibrium between the OLDA adsorption and the corrosion process starts from about 30 min of immersion in agreement with the inhibition efficiency variation.

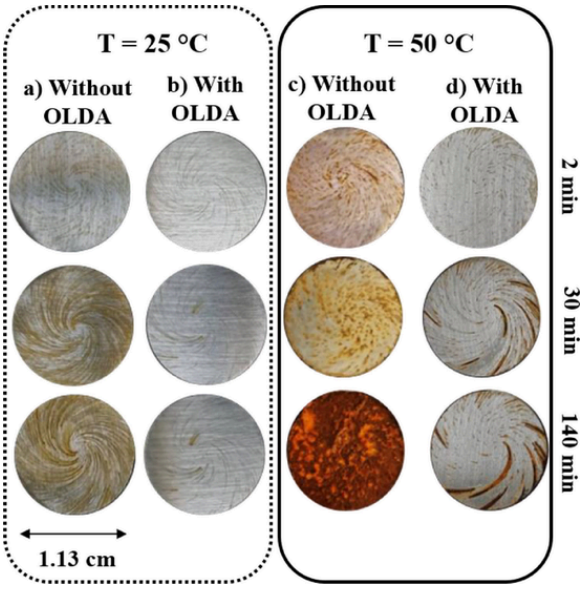

Fig. 6. Ex situ observations of the carbon steel electrode surface (1 cm^2) in a 200 $mg.kg^{-1}$ NaCl solution with and without OLDA at 25°C and 50°C after 2 min, 30 min and 140 min of immersion (from top to bottom). Electrode rotation rate: 500 rpm.

3.1.4. Capacitance variation

The OLDA adsorption can be directly investigated by transforming the impedance data at high frequency into capacitance [21–26]. In the present work, the capacitance values were calculated at different frequencies according to Eq. (4):

$$C'(\omega) = \frac{-Z_j}{\omega\left[\left(Z_r - R_e\right)^2 + \left(Z_j\right)^2\right]} \quad (4)$$

where Z_r and Z_j are the real and imaginary parts of the impedance; ω is the angular frequency and R_e is the electrolyte resistance. The obtained capacitance variations were similar independently of the chosen frequency. As an example, Fig. 7 shows the capacitance values, calculated at 300 Hz, at 25°C and 50°C as a function of immersion time.

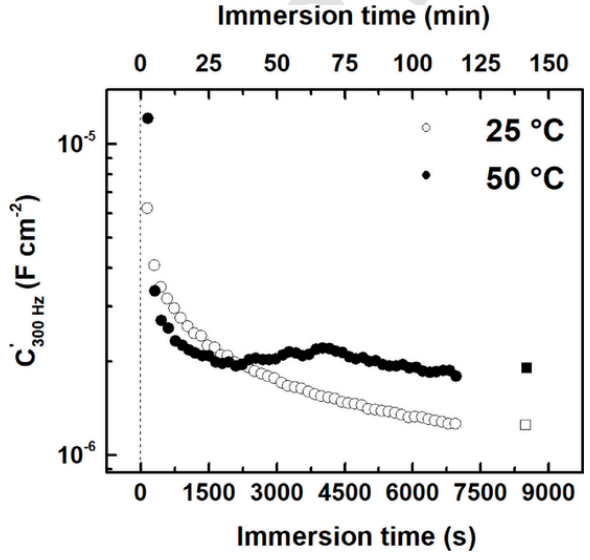

Fig. 7. Capacitance variation at 300 Hz as a function of immersion time at 25°C (○) and 50°C (●). The last points correspond to the complete spectra after 140 min of immersion at 25°C (□) and 50°C (■).

At 25°C, the capacitance decrease is progressive until its stabilization. The capacitance variation confirms the correlation of the OLDA adsorption and its inhibition efficiency [14]. At 50°C, the capacitance decreases more rapidly during the first 25 min suggesting a faster OLDA adsorption onto the surface than at 25°C. With temperature increase, the solubility and mobility of OLDA molecules in the NaCl solution might increase, favoring a faster adsorption [41]. After 30 min, the capacitance variation undergoes some fluctuations. The fluctuations correspond to the time frame (30-75 min) for which the inhibition efficiency decreased. It is likely that the corrosion rate speeds up during this time frame, resulting in a partial desorption of the OLDA molecules from the surface [26]. Steady-state is however reached from 75 min of immersion until the end of the experiment. To investigate the distribution and the possible interaction of the OLDA molecules with the corrosion products, *ex situ* Raman spectroscopy and PM-IRRAS analyses were performed.

3.2. Ex situ surface characterization

3.2.1. Raman spectroscopy analysis

A spot of the carbon steel surface (40 × 50 μm) (Fig. 6b) in presence of OLDA at 25°C and after 140 minutes of immersion is shown in Fig. 8a. This spot shows corroded and apparent un-corroded areas. To obtain the OLDA distribution on these areas (map of the spot in Fig. 8b), the bands representative of either the OLDA molecules or corrosion products were used. As an example, a Raman spectrum on the corroded area in presence of OLDA is shown in Fig. 8c. For comparison, a spectrum of the corrosion products formed in absence of OLDA and the bulk OLDA are shown in Fig. 8d and Fig. 8e, respectively.

Raman spectrum on the corroded area (Fig. 8c) exhibits the following bands at: 234, 249, 378, 525, 643, 1054 and 1300 cm^{-1}, corresponding mainly to lepidocrocite (γ-FeOOH) [49–53]. The same iron hydroxide phase was formed on the carbon steel surface in absence of OLDA at 25°C and after 140 min of immersion (Fig. 8d). The Raman spectrum in Fig. 8c also reveals the presence of several bands between 2800-3000 cm^{-1} and one band at 3004 cm^{-1} corresponding to the symmetric ($\nu_s CH_2$) and antisymmetric ($\nu_a CH_2$) stretching mode of methylene groups and to the ethylenic elongation ($\nu CH(C=C)$), respectively. The bands at about 1445 cm^{-1} and 1650 cm^{-1} correspond to the methylene deformation mode (δCH_2) and the bending modes of NH_2 and NH groups, respectively. The presence of these bands, as compared to the bulk OLDA spectrum (Fig. 8e) attests the OLDA adsorption onto the corrosion products.

The νCH_2 (OLDA) signal in green and A_{1g} (γ-FeOOH) signal in red (Fig. 8c) allow the OLDA and hydroxides distribution on the mapped spot to be followed. The heterogeneity in the distribution of OLDA is clearly visible. In domains (1) and (2) (Fig. 8b), the OLDA presence predominates over the iron hydroxide. The intermediate yellow color in domain (3) indicates that OLDA and corrosion products co-exist. The apparent un-corroded area is black because of a missing Raman signal due to a smaller adsorbed OLDA quantity. However, no traces of oxide were detected in the same area suggesting indirectly the OLDA adsorption. Yoshioka et al. [13] have noted, by IR microscopy, the same heterogeneous distribution of OLDA barrier formed at 150°C along a copper surface.

Additional analyses (data not shown) at 50°C and after 140 min of immersion showed that the predominant formed iron hydroxide phase (γ-FeOOH) does not vary with temperature increase or in presence of OLDA. The latter is heterogeneously distributed onto the surface and preferentially adsorbed onto the corrosion products.

3.2.2. PM-IRRAS analysis

The PM-IRRAS analyses were carried out for an ellipsoidal spot of 6 mm × 2 mm, including mostly an apparent un-corroded area, and for short immersion times: 2 min, 10 min and 30 min at 25°C and 2 min and

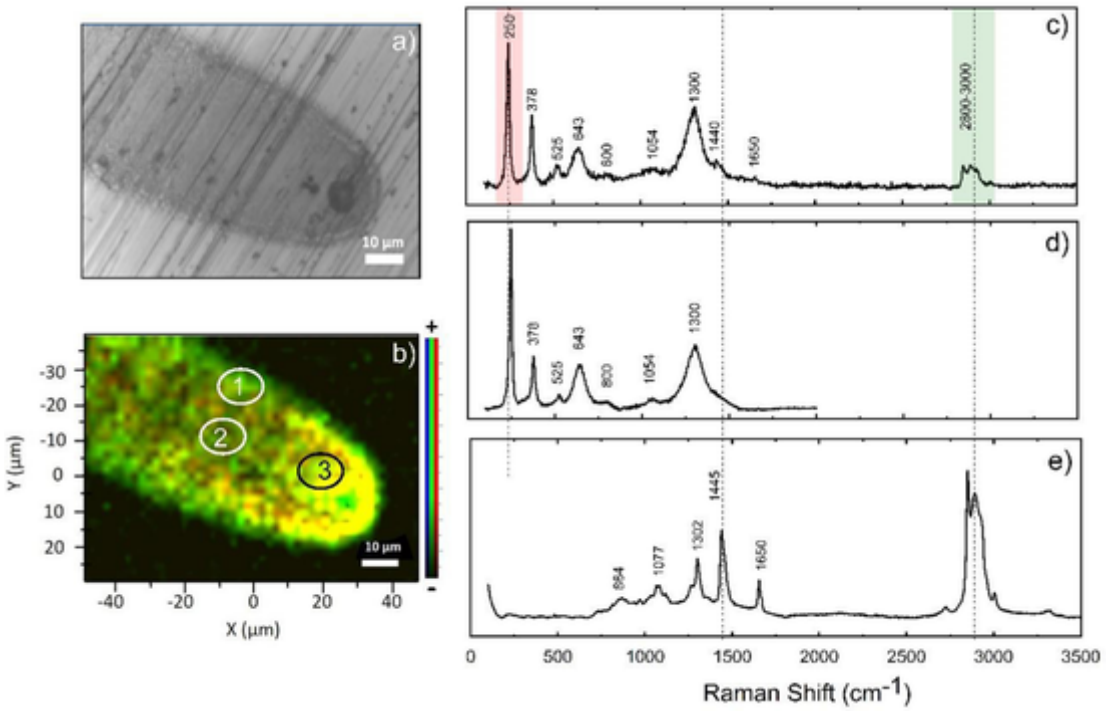

Fig. 8. . a) Micrograph of the mapped surface area at 25°C. b) Raman image of the νCH_2 (OLDA) and A_{1g} (γ-FeOOH) band distribution. c) Raman spectrum on the corroded area. d) Raman spectrum of corrosion products formed in absence of OLDA at 25°C after 140 min of immersion. e) Raman spectrum of bulk OLDA.

5 min at 50°C (Fig. 9). The IRRAS spectra show the presence of two intense bands in the 3000-2800 cm^{-1} range, related to the asymmetric ($\nu_a CH_2$) and symmetric ($\nu_s CH_2$) stretching modes of methylene groups at 2926 cm^{-1} and 2854 cm^{-1}, respectively. A weak band is also observed at 3004 cm^{-1}, related to the νCH stretching mode of unsaturated C=C bond. In the 1700-1500 cm^{-1} range, an unusual pattern is observed with four contributions at 1680, 1640, 1588 and 1545 cm^{-1}. Since ATR spectrum of OLDA (data not shown) revealed only two bands at around 1650 and 1600 cm^{-1} for the bending modes of the NH_2 and NH groups, respectively, it is clear that other species should be formed on the steel surface. Equilibrium between the protonated and unprotonated forms of the NH_2 or NH groups could be a possibility as well as the formation of –NH–COO^- group, as previously reported by Oviedo *et al.* [54]. In their work, the presence of the carbamate on mica surface has been explained by the fast reaction between ODA molecules and dissolved CO_2 in water. The band related to the bending mode of methylene groups (δCH_2) is observed at 1465 cm^{-1}, while two weak bands are also present at 1377 and 1323 cm^{-1}, due to the wagging modes (ωCH_2). Finally, the band at 1020 cm^{-1} confirms the lepidocrocite γ-FeOOH iron phase formation [55–56] for the studied conditions. These first results validate the EIS study conclusions as for the OLDA adsorption as soon as 2 min of immersion for both temperatures.

The IRRAS intensity of the $\nu_a CH_2$ band increases with immersion time at 25°C and 50°C. In addition, the IRRAS intensity of the $\nu_a CH_2$ band for the all the samples at 50°C is higher than those at 25°C. OLDA barrier thicknesses can be estimated from the experimental data. For 2 min, 10 min and 30 min of immersion at 25°C, thicknesses of 4 nm, 9 nm and 12 nm were obtained, respectively. For 2 min and 5 min of immersion at 50°C, thicknesses of 16 nm and 20 nm were determined, respectively. The increase of the IRRAS intensity of $\nu_a CH_2$ band is accompanied by the increase of the lepidocrocite band intensity at 1020 cm^{-1}. It is thusly crucial to note that the provided thicknesses (only meaningful for isotropic and compact arrangement of organic molecules onto substrate) should not be considered for their absolute values but more

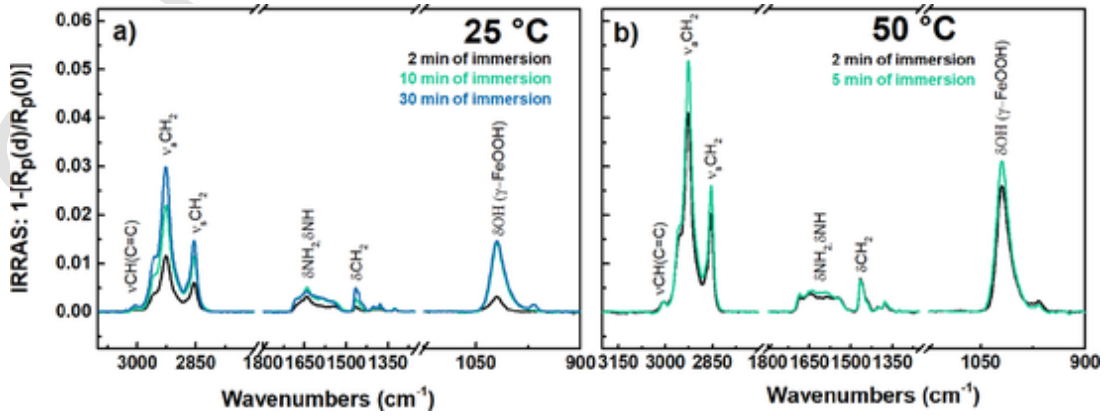

Fig. 9. . a) IRRAS spectra of OLDA barrier formed onto the carbon steel for 2 min, 10 min and 30 min of immersion at 25°C into a 100 $mg.kg^{-1}$ OLDA / 200 $mg.kg^{-1}$ NaCl solution b) 2 min and 5 min of immersion at 50°C.

as an order of magnitude of the adsorbed OLDA molecules. The estimated thicknesses values are higher than that of a monolayer and in agreement with those previously reported in literature [7-8, 12-13]. The theoretical thickness of an OLDA monolayer by considering an adsorption with both amine functions is 2.1 nm (the length of the alkyl carbon chain) or lower depending on the arrangement of the molecules on the surface. We attribute the accumulation of OLDA molecules to the formation of mixed layers OLDA/corrosion products.

To confirm the role of corrosion products on the mixed layers formation, PM-IRRAS analyses were conducted on gold substrate for 30 min of immersion at 25°C and 10 min, 30 min and 90 min of immersion at 50°C.

The IRRAS spectra (Fig. 10) exhibit the same bands as for the carbon steel surface with the exception of the band at 1020 cm^{-1} confirming that there are not any oxides present. The ν_aCH_2 band does not vary as a function of time nor temperature. Furthermore, the observed IRRAS intensity of the ν_aCH_2 band is lower than those of the adsorbed OLDA onto the carbon steel surface. A thickness of about 1.2 nm was revealed from the IRRAS intensity of ν_aCH_2 mode. The value is similar to the ODA thickness (1.5-1.7 nm) determined on model surfaces such as mica by AFM and ATR-FTIR [54, 57].

In conclusion, the formation of hydroxides favours the accumulation of OLDA molecules. The increased hydrophilicity due to the presence of –OH groups can promote the interaction between the surface and the amines [58]. The incorporation of OLDA molecules into the corrosion products could form coordination complexes leading to mixed layers OLDA/corrosion products.

Furthermore, it can be noted that for all the studied conditions on the carbon steel and gold surfaces, the wavenumbers of ν_aCH_2 and ν_sCH_2 bands at 2926 and 2854 cm^{-1}, respectively, indicate gauche defects in the alkyl chains of the OLDA molecule [34]. The OLDA molecules are therefore disordered on the surface in agreement with Yoshioka *et al.* conclusions [13].

4. Conclusions

In the present work, a methodology was proposed combining *in situ* EIS and *ex situ* PM-IRRAS and Raman spectroscopy techniques for monitoring FFAs adsorption and corrosion kinetics onto carbon steel surface in neutral aerated conditions at 25°C and 50°C. EIS measurements were recorded from 20 s of immersion and every 140 s for a total duration of 2 h. The variations of the inhibition efficiency and of the FFAs barrier capacitance were examined over immersion time. It was found that the OLDA adsorption and the corrosion process occurred simultaneously onto the carbon steel surface. The first calculated inhibition efficiency (2 min) for both temperatures was around 50 % confirming the instantaneous adsorption of OLDA onto the carbon steel surface. Raman spectroscopy surface analyses revealed that OLDA was adsorbed heterogeneously on the carbon steel surface with a preferential adsorption onto the corrosion products (mainly γ-FeOOH). PM-IRRAS analysis allowed the OLDA barrier thickness over immersion time to be estimated. The *ex situ* analysis showed that OLDA adsorption and corrosion of carbon steel surface started simultaneously from 2 min of immersion corroborating the EIS results. More OLDA molecules and more corrosion products were accumulated onto the carbon steel surface with increasing immersion time and temperature. By using gold substrate as a model surface, it was shown that OLDA molecules do not accumulate in absence of corrosion products. The study confirmed the significant role played by the corrosion products on the FFAs adsorption process. This methodology may be considered to investigate adsorption kinetics of other FFAs substances or for different physical-chemical conditions such as pH, FFAs concentration, oxygen level, medium conductivity, temperature and pressure.

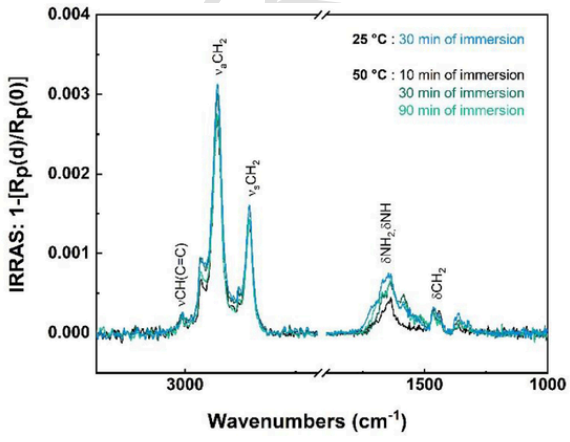

Fig. 10. IRRAS spectra of adsorbed OLDA onto gold surface after 30 min of immersion at 25°C and 10 min, 30 min and 90 min of immersion at 50°C into a 100 $mg.kg^{-1}$ OLDA / 200 $mg.kg^{-1}$ NaCl solution.

CRediT authorship contribution statement

Deni Jero: Conceptualization, Data curation, Formal analysis, Investigation, Methodology, Writing - original draft. **Nicolas Caussé:** Conceptualization, Formal analysis, Investigation, Methodology, Project administration, Supervision, Validation, Writing - review & editing. **Olivier Marsan:** Investigation, Writing - review & editing. **Thierry Buffeteau:** Investigation, Writing - review & editing. **Fabrice Chaussec:** Project administration, Resources, Supervision, Writing - review & editing. **Amaury Buvignier:** Project administration, Resources, Supervision, Writing - review & editing. **Marion Roy:** Project administration, Supervision, Validation, Writing - review & editing. **Nadine Pébère:** Conceptualization, Formal analysis, Investigation, Methodology, Project administration, Supervision, Validation, Writing - review & editing.

Data availability

The raw/processed data required to reproduce these findings cannot be shared at this time as the data also forms part of an ongoing study.

Declaration of Competing Interest

The authors declare that they have no known competing financial interests or personal relationships that could have appeared to influence the work reported in this paper.

Data Availability

Data will be made available on request.

References

[1] E. Bardal, Corrosion and protection, Springer, 2004, https://doi.org/10.1007/b97510.
[2] I. Betova, M. Bojinov, T. Saario, Film-forming amines in steam /water cycles – structure, properties, and influence on corrosion, VTT-R-0323 (2014) 1-41.
[3] E. Chernyshev, E. Veprov, V. Petrov, S. Bogdanov, T. Levina, T. Petrova, V. Kashinskii, A. Zonov, A. Verkhovskii, Increasing the corrosion resistance of equipment due to the use of film-forming amines, Power Technol. Eng. 40 (2006) 34–37, https://doi.org/10.1007/s10749-006-0016-6.
[4] R. Wagner, E. Czempik, Experience in preservation of the water steam cycle in CCPP (Combined Cycle Power Plants) with ODA (Octadecylamine), J. Energy Power Eng. 10 (2016) 32–38, https://doi.org/10.17265/1934-8975/2016.01.004.
[5] B. Smith, P. McCann, K. Uchida, S. Mori, J. Jasper, W. Hater, Determination of Oleyl Propylenediamine, a commonly used film forming amine, on the surfaces of water-steam cycles, Powerpl. Chem. 19 (2017) 129–140.
[6] W. Hater, B. Smith, P. Mccann, A. De Bache, Experience with the application of a film forming amine in the Connah's quay triple stage combined cycle gas turbine power plant operating in cycling mode, Powerpl. Chemistry 20 (2018) 136–144.
[7] J. Baux, N. Caussé, J. Esvan, S. Delaunay, J. Tireau, M. Roy, D. You, N. Pébère,

Impedance analysis of film-forming amines for the corrosion protection of a carbon steel, Electrochim. Acta 283 (2018) 699–707, https://doi.org/10.1016/j.electacta.2018.06.189.
[8] J. Baux, N. Caussé, S. Delaunay, J. Tireau, M. Roy, D. You, N. Pébère, Film-forming amines for the corrosion protection of carbon steels in nuclear power plant secondary circuit conditions: an impedance study, J. Electrochem. Soc. 167 (2020), https://doi.org/10.1149/1945-7111/ab7d42.
[9] H. Topp, W. Hater, A. De Bache, C. zum Kolk, Film-forming amines in shell boilers, Powerpl. Chem. 14 (2012) 38–48.
[10] F. Mao, C. Dong, D.D. Macdonald, Effect of octadecylamine on the corrosion behavior of Type 316SS in acetate buffer, Corros. Sci. 98 (2015) 192–200, https://doi.org/10.1016/j.corsci.2015.05.022.
[11] Z. Liu, B. Lv, D. Wu, Y. Sun, Morphology and magnetic properties of α-Fe_2O_3 particles prepared by octadecylamine-assisted hydrothermal method, Particuology 10 (2012) 456–461, https://doi.org/10.1016/j.partic.2011.11.012.
[12] E. Jäppinen, T. Ikäläinen, S. Järvimäki, T. Saario, K. Sipilä, M. Bojinov, Corrosion behavior of carbon steel coated with octadecylamine in the secondary circuit of a pressurized water reactor, J. Mater. Eng. Perform. 26 (2017) 6037–6046, https://doi.org/10.1007/s11665-017-3035-6.
[13] H. Yoshioka, K. Yoshida, N. Noguchi, T. Ueki, K.-i. Murai, K. Watanabe, M. Nakahara, Microscopic structure and binding mechanism of the corrosion-protective film of Oleylpropanediamine on copper in hot water, J. Phys. Chem. C 126 (2022) 6436–6447, https://doi.org/10.1021/acs.jpcc.2c00526.
[14] Y. Zhu, M.L. Free, R. Woollam, W. Durnie, A review of surfactants as corrosion inhibitors and associated modeling, Prog. Mater. Sci. 90 (2017) 159–223, https://doi.org/10.1016/j.pmatsci.2017.07.006.
[15] M. Jack, S. Weerakul, D.H. Lister, The interaction of a film-forming amine with surfaces of a recirculating experimental water loop, in: Proc. Int. Conf. Heat Exch. Fouling Clean, 2015, pp. 112–118.
[16] F. Cuoq, J. Benguigui, C. Geijselaers, F. Lampert, Linking thermoelectric effect and adsorption of film forming amine as a corrosion inhibitor for industrial systems, Ind. Eng. Chem. Res. 95 (2020) 8492–8495, https://doi.org/10.1021/acs.iecr.0c00576.
[17] S. Marcelin, N. Pébère, Synergistic effect between 8-hydroxyquinoline and benzotriazole for the corrosion protection of 2024 aluminium alloy: A local electrochemical impedance approach, Corros. Sci. 101 (2015) 66–74, https://doi.org/10.1016/j.corsci.2015.09.002.
[18] N. Ochoa, F. Moran, N. Pébère, The synergistic effect between phosphonocarboxylic acid salts and fatty amines for the corrosion protection of a carbon steel, J. Appl. Electrochem. 34 (2004) 487–493, https://doi.org/10.1023/B:JACH.0000021702.49827.11.
[19] P. Bommersbach, C. Alemany-Dumont, J. Millet, B. Normand, Hydrodynamic effect on the behaviour of a corrosion inhibitor film: Characterization by electrochemical impedance spectroscopy, Electrochim. Acta 51 (2006) 4011–4018, https://doi.org/10.1016/j.electacta.2005.11.020.
[20] M.P. Desimone, G. Grundmeier, G. Gordillo, S.N. Simison, Amphiphilic amido-amine as an effective corrosion inhibitor for mild steel exposed to CO_2 saturated solution: Polarization, EIS and PM-IRRAS studies, Electrochim. Acta 56 (2011) 2990–2998, https://doi.org/10.1016/j.electacta.2011.01.009.
[21] R. Subramanian, V. Lakshminarayanan, Study of kinetics of adsorption of alkanethiols on gold using electrochemical impedance spectroscopy, Electrochim. Acta 45 (2000) 4501–4509, https://doi.org/10.1016/S0013-4686(00)00512-0.
[22] U.K. Sur, R. Subramanian, V. Lakshminarayanan, Cyclic voltammetric and electrochemical impedance studies on the structure, adsorption kinetics, and barrier properties of some organic dithiol self-assembled monolayers on gold, J. Colloid Interface Sci. 266 (2003) 175–182, https://doi.org/10.1016/S0021-9797(03)00568-X.
[23] S. Shrikrishnan, K. Sankaran, V. Lakshminarayanan, Electrochemical impedance analysis of adsorption and enzyme kinetics of calf intestine alkaline phosphatase on SAM-modified gold electrode, J. Phys. Chem. 116 (2012) 16030–16037, https://doi.org/10.1021/jp3027463.
[24] V.S. Dilimon, S. Rajalingam, J. Delhalle, Z. Mekhalif, Self-assembly mechanism of thiol, dithiol, dithiocarboxylic acid, disulfide and diselenide on gold: an electrochemical impedance study, Phys. Chem. Chem. Phys. 15 (2013) 16648, https://doi.org/10.1039/C3CP51804C.
[25] V.S. Dilimon, G. Fonder, J. Delhalle, Z. Mekhalif, Self-assembled monolayer formation on copper: A real time electrochemical impedance study, J. Phys. Chem. C 115 (2011) 18202–18207, https://doi.org/10.1021/jp203652y.
[26] V.S. Dilimon, J. Denayer, J. Delhalle, Z. Mekhalif, Electrochemical and spectroscopic study of the self-assembling mechanism of normal and chelating alkanethiols on copper, Langmuir 28 (2012) 6857–6865, https://doi.org/10.1021/la300021g.
[27] S.C. Medina, A.S.F. Farinha, A.-H. Emwas, A. Tabatabai, T. Leiknes, A fundamental study of adsorption kinetics of surfactants onto metal oxides using quartz crystal microbalance with dissipation (QCM-D), Colloids Surfaces A Physicochem. Eng. Asp. 586 (2020) 124237, https://doi.org/10.1016/j.colsurfa.2019.124237.
[28] D. Wang, X. Tang, Y. Qiu, F. Gan, G. Zheng Chen, A study of the film formation kinetics on zinc in different acidic corrosion inhibitor solutions by quartz crystal microbalance, Corros. Sci. 47 (2015) 2157–2172, https://doi.org/10.1016/j.corsci.2004.10.003.
[29] F. Damos, R.C.S. Luz, L.T. Kubota, Determination of thickness, dielectric constant of thiol films, and kinetics of adsorption using surface plasmon resonance, Langmuir 21 (2005) 602–609, https://doi.org/10.1021/la0487038.
[30] C. Tamerler, E.E. Oren, M. Duman, E. Venkatasubramanian, M. Sarikaya, Adsorption kinetics of an engineered gold binding peptide by surface plasmon resonance spectroscopy and a quartz crystal microbalance, Langmuir 22 (2006) 7712–7718, https://doi.org/10.1021/la0606897.
[31] A.T. Tran, F. Huet, K. Ngo, P. Rousseau, Artefacts in electrochemical impedance measurement in electrolytic solutions due to the reference electrode, Electrochim. Acta 56 (2011) 8034–8039, https://doi.org/10.1016/j.electacta.2010.12.088.
[32] T. Buffeteau, B. Desbat, J. Turlet, Polarization modulation FT-IR spectroscopy of surfaces and ultra-thin films: experimental procedure and quantitative analysis, Appl. Spectrosc. 45 (1991) 380–389, https://doi.org/10.1366/0003702914337308.
[33] T. Buffeteau, B. Desbat, D. Blaudez, J. Turlet, Calibration procedure to derive IRRAS spectra from PM-IRRAS spectra, Appl. Spectrosc. 54 (200) 1646-1650, https://doi.org/10.1366/0003702001948673.
[34] E.D. Palik, Handbook of optical constants of solids, Academic press, 1998.
[35] F. Abelès, Sur la propagation des ondes électromagnétiques dans les milieux stratifiés, Ann. Phys. 12 (1948) 504–520, https://doi.org/10.1051/anphys/194812030504.
[36] T. Buffeteau, B. Desbat, Thin-film optical constants determined from infrared reflectance and transmittance measurements, Appl. Spectrosc. 43 (1989) 1027–1032, https://doi.org/10.1366/0003702894203813.
[37] K. Yamamoto, H. Ishida, Interpretation of reflection and transmission spectra for thin films: reflection, Appl. Spectrosc. 48 (1994) 775–787, https://doi.org/10.1366/0003702944029839.
[38] M. Dignam, S. Mamiche-Afara, Determination of the spectra of the optical constants of bulk phases via Fourier transform ATR, Spectrochim. Acta Part A Mol. Spectrosc. 44 (1988) 1435–1442, https://doi.org/10.1016/0584-8539(88)80195-8.
[39] E. Siurdyban, T. Brotin, K. Heuzé, L. Vellutini, T. Buffeteau, Immobilization of cryptophane derivatives onto SiO/Au and Au substrates, Langmuir 30 (2014) 14859–14867, https://doi.org/10.1021/la5039156.
[40] M. Ameer, E. Khamis, G. Al-Senani, Effect of temperature on stability of adsorbed inhibitors on steel in phosphoric acid solution, J. Appl. Electrochem. 32 (2002) 149–156, https://doi.org/10.1023/A:1014777726624.
[41] B. Jiang, W. Sun, J. Cai, S. Chen, B. Hou, Inhibition of carbon steel corrosion in HCl solution using N-oleyl-1,3-propanediamine based formulation, Colloids Surfaces A Physicochem. Eng. Asp. 624 (2021) 126824, https://doi.org/10.1016/j.colsurfa.2021.126824.
[42] M. Sancy, Y. Gourbeyre, E. Sutter, B. Tribollet, Mechanism of corrosion of cast iron covered by aged corrosion products: application of electrochemical impedance spectrometry, Corros. Sci. 52 (2010) 1222–1227, https://doi.org/10.1016/j.corsci.2009.12.026.
[43] M. Hitchman, Measurement of dissolved oxygen, Wiley and Sons, New York, 1978.
[44] S. Tierce, N. Pébère, C. Blanc, C. Casenave, G. Mankowski, H. Robidou, Corrosion behaviour of brazing material AA4343, Electrochim. Acta 52 (2006) 1092–1100, https://doi.org/10.1016/j.electacta.2006.07.007.
[45] D. You, N. Pébère, F. Dabosi, An investigation of the corrosion of pure iron by electrochemical techniques and in situ observations, Corros. Sci. 34 (1993) 5–15, https://doi.org/10.1016/0010-938X(93)90254-E.
[46] T. De Seranno, E. Lambrechts, E. De Meyer, W. Hater, N. De Geyter, A.R. Verliefde, T. Depover, K. Verbeken, Effect of film-forming amines on the acidic stress-corrosion cracking resistance of steam turbine steel, Metals 10 (2020) 1–20, https://doi.org/10.3390/met10121628.
[47] A. Lasia, Electrochemical Impedance Spectroscopy and its Applications, Springer, 2014, https://doi.org/10.1007/978-1-4614-8933-7.
[48] M.S. Walczak, P. Morales-Gil, R. Lindsay, Determining Gibbs energies of adsorption from corrosion inhibition efficiencies: Is it a reliable approach? Corros. Sci. 155 (2019) 182–185, https://doi.org/10.1016/j.corsci.2019.04.040.
[49] J. Dünnwald, A. Otto, An investigation of phase transitions in rust layers using Raman spectroscopy, Corros. Sci. 29 (1989) 1167–1176, https://doi.org/10.1016/0010-938X(89)90052-8.
[50] S.J. Oh, D. Cook, H. Townsend, Characterization of iron oxides commonly formed as corrosion products on steel, Hyperfine Interact 112 (1998), https://doi.org/10.1023/A:1011076308501.
[51] D. L. A. de Faria, S. Venaüncio Silva, M.T. de Oliveira, Raman microspectroscopy of some iron oxides and oxyhydroxides, J. Raman Spectrosc. 28 (1997) 873-878, https://doi.org/10.1002/(SICI)1097-4555(199711)28:11%3C873::AID-JRS177%3E3.0.CO;2-B.
[52] C. Thinaharan, R.P. George, J. Philip, *In situ* Raman spectroscopic analysis on carbon steel, immersed in aqueous solutions at different pH and anions, J. Mater. Eng. Perform. 29 (2020) 2792–2805, https://doi.org/10.1007/s11665-020-04805-x.
[53] T. Ohtsuka, K. Kubo, N. Sato, Raman spectroscopy of thin corrosion films on iron at 100 to 150°C in air, Corrosion 42 (1986) 476–481, https://doi.org/10.5006/1.3583054.
[54] J. Oviedo, M.A. San-Miguel, J.A. Heredia-Guerrero, J.J. Benítez, Electrostatic induced molecular tilting in self-assembled monolayers of n-octadecylamine on mica, J. Phys. Chem. C 116 (2012) 7099–7105, https://doi.org/10.1021/jp300829g.
[55] H. Namduri, S. Nasrazadani, Quantitative analysis of iron oxides using Fourier transform infrared spectrophotometry, Corros. Sci. 50 (2008) 2493–2497, https://doi.org/10.1016/j.corsci.2008.06.034.
[56] D.G. Lewis, V.C. Farmer, Infrared absorption of surface hydroxyl groups and lattice vibrations in lepidocrocite (γ-FeOOH) and boehmite (γ-AlOOH), Clay Miner 1 (1986) 93–100, https://doi.org/10.1180/claymin.1986.021.1.08.
[57] S. Campen, J.H. Green, G. Lamb, H. Spikes, In situ study of model organic friction modifiers using liquid cell AFM: Self-assembly of octadecylamine, Tribol. Lett. 58

(2015), https://doi.org/10.1007/s11249-015-0514-5.
[58] C. Gadois, J. Światowska, S. Zanna, P. Marcus, Influence of titanium surface treatment on adsorption of primary amines, J. Phys. Chem. C 117 (2013) 1297–1307, https://doi.org/10.1021/jp306786w.